INVITED PAPER *Joint Special Section on Opto-electronics and Communications for Future Optical Network*

Broadband Port-Selective Silicon Beam Scanning Device for Free-Space Optical Communication

Yuki ATSUMI[†a)], **Tomoya YOSHIDA**[†], **Ryosuke MATSUMOTO**[†], **Ryotaro KONOIKE**[†], ***Members***,
Youichi SAKAKIBARA[†], ***Nonmember***, **Takashi INOUE**[†], ***and*** **Keijiro SUZUKI**[†], ***Members***

SUMMARY Indoor free space optical (FSO) communication technology that provides high-speed connectivity to edge users is expected to be introduced in the near future mobile communication system, where the silicon photonics solid-state beam scanning device is a promising tool because of its low cost, long-term reliability, and other beneficial properties. However, the current two-dimensional beam scanning devices using grating coupler arrays have difficulty in increasing the transmission capacity because of bandwidth regulation. To solve the problem, we have introduced a broadband surface optical coupler, "elephant coupler," which has great potential for combining wavelength and spatial division multiplexing technologies into the beam scanning device, as an alternative to grating couplers. The prototype port-selective silicon beam scanning device fabricated using a 300 mm CMOS pilot line achieved broadband optical beam emission with a 1 dB-loss bandwidth of 40 nm and demonstrated beam scanning using an imaging lens. The device has also exhibited free-space signal transmission of non-return-to-zero on-off-keying signals at 10 Gbps over a wide wavelength range of 60 nm. In this paper, we present an overview of the developed beam scanning device. Furthermore, the theoretical design guidelines for indoor mobile FSO communication are discussed.

key words: *silicon photonics, beam scanning devices, Indoor free-space optical communication, surface optical coupler, optical switches*

1. Introduction

Free-space optical (FSO) communication is a promising technology for enabling high-capacity signal transmission between stations and devices where it is difficult to install optical fiber networks. Notably, there is a wide range of potential applications for FSO communication, including communication between satellites, self-driving cars, high-speed trains, infrastructure, buildings, and rack-to-rack communication in a data center [1]. Especially in the next-generation mobile optical communication systems that will go beyond 5G and 6G, FSO is expected to play an important role to provide ultra-high capacity, ultra-multiple connections, and ultra-low latency data transmission to edge users [2]. In these systems, FSO communication using near-infrared laser light is more suitable for mobile access than traditional radio frequency (RF) and visible light communication using illumination systems because of several advantages such as broad bandwidth, license-free bandwidth, eye-safe wavelength, connectivity with optical fiber networks in buildings, and privacy protection [1], [3]–[9]. Considering such mobile optical communication systems, laser safety regulations will prohibit FSO signal transmission with high enough power to fully cover the user area using a single spreading light [8]. Therefore, to maintain a constant connection with the moving users, optical signal-pointing technology using optical beam scanning devices is required, in addition to user-localized and tracking technologies using RF and image-sensing systems [1].

Among several beam scanning approaches [1], [9], [10], solid-state beam scanning devices based on silicon photonics have been actively developed for image sensing and light detection and ranging applications, as well as FSO communications. The reason is that silicon (Si) photonics uses mature CMOS technology and has multiple advantages such as mass-producibility, low cost, compactness, low-energy-consumption, high-speed-response, and robustness [3], [4], [11]–[15]. In Si photonics devices, grating couplers or chip-edge couplers are typically used as the optical emitter [16]–[19]. However, the grating coupler has difficulty increasing the transmission capacity because of the limited bandwidth, and the edge coupler has difficulty in two-dimensional (2D) beam scanning. Therefore, it is challenging to simultaneously achieve 2D beam scanning and broadband communication in Si photonics devices.

To solve the problem, we have developed a broadband 2D silicon beam scanning device by installing chip-surface optical couplers, "elephant couplers," which consist of three parts: a vertically curved Si wire waveguide, short silicon inversed taper, and dome-like SiO_2 coupler top, as shown in Fig. 1 [20], [21]. Elephant couplers feature low-loss and broadband optical coupling perpendicular to the chip surface, and thus, are suitable for wavelength division multiplexing (WDM) and spatial division multiplexing (SDM) systems [20]–[28]. The developed scanning device contains a tournament-tree arranged Mach-Zehnder (MZ) optical switch circuit and elephant coupler arrays, where an imaging lens was installed above the device chip to deflect the output optical beams from each optical coupler. The fabricated device exhibited broadband optical coupling operation with a 1dB-loss bandwidth of 40 nm. Furthermore, beam scanning operation and free-space transmission of non-return-to-zero on-off-keying (NRZ-OOK) signals at 10 Gbps were demonstrated in the wide wavelength range from 1530 to 1590 nm [21]. To the best of our knowledge, this is the first report of free-space signal transmission in such a wide wavelength range using a 2D silicon photonics beam scanning device.

Manuscript received December 19, 2022.
Manuscript revised March 5, 2023.
Manuscript publicized May 24, 2023.
[†]The authors are with AIST, Tsukuba-shi, 305–8568 Japan.
a) E-mail: y-atsumi@aist.go.jp
DOI: 10.1587/transele.2022OCI0001

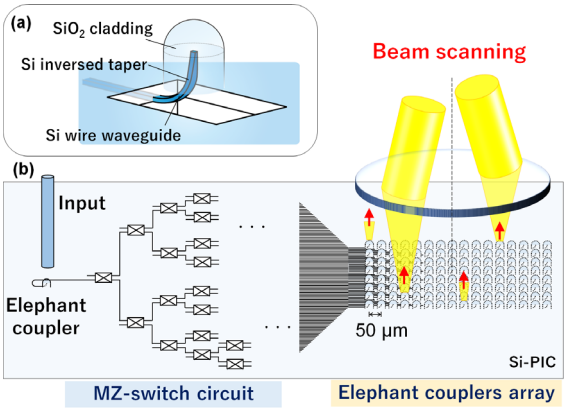

Fig. 1 Schematic images: (a) Elephant coupler. (b) Proposed port-selective silicon beam scanner.

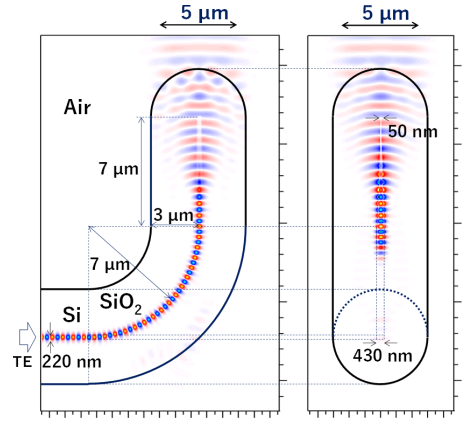

Fig. 2 Electric field profile for TE-like mode propagation in an elephant coupler at a wavelength of 1550 nm [24].

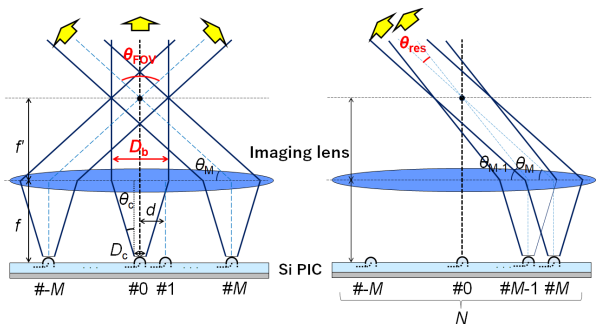

Fig. 3 Schematic image of the beam scanning operation.

In this paper, we present an overview of the developed beam scanning device including the design guidelines for indoor mobile FSO communications. This paper complements the contents of the conference proceedings [20], [21], and a more detailed discussion is held according to the design guidelines.

The rest of this paper is organized as follows. First, in Sect. 2, we present the design guidelines for beam scanning devices based on indoor mobile FSO communications. Then, we show the design and fabrication of the beam scanner in Sect. 3. Furthermore, we discuss the experimental results of optical characterization and signal transmission in Sect. 4.

2. Theoretical Analysis of the Beam Scanning System

2.1 Elephant Coupler

Figure 2 depicts the electric field profile for TE-like mode propagation in an elephant coupler calculated using a three-dimensional finite difference time domain method, in which the taper length and SiO_2 radius are 7 and 3 μm, respectively [25]. The light propagating in the silicon planer optical circuit changes the propagating direction perpendicular to the chip surface along the vertically curved waveguide. It then diverges drastically into the surrounding SiO_2 cladding through the short inverse taper, and the diverged light reaching the coupler top is quasi-collimated by the dome-like SiO_2 structure with a beam spot size of 5 μm and is output to the free space. Using this approach, the elephant coupler can efficiently enlarge the output beam spot size in a small device footprint. Furthermore, the wavelength sensitivity is small because the direction of light propagation is changed through the bent waveguide, and a small polarization-dependent-loss coupling operation can be achieved depending on the design [25], [27].

Previously, we have successfully developed broadband, low-loss, and low-polarization-sensitivity optical couplers with beam spot sizes of 5 and 10 μm [25], [27]. Furthermore, we have demonstrated an optical orbital angular momentum (de)multiplexer by arranging the couplers in a small circle [28]. Thus, the elephant coupler exhibits efficient coupling performance and two-dimensional integration and is suitable for merging WDM and SDM systems.

2.2 Operating Mechanism of the Beam Scanner

The silicon photonics beam scanning devices are categorized into the optical phased array approach [3], [4], [13] and the port-selective approach using optical lens deflection [11], [12], [14], [15], [20], [21]. The former controls the beam direction by applying phase difference to each light emitting from the optical coupler array and interfering with them in free space. Although the beam vector can be steered analogously, integration of many optical couplers in a short pitch (half of the wavelength) is required to suppress unnecessary sidelobes. Furthermore, precise phase control is required for all optical paths. Conversely, the latter approach deflects the single beam output from the selected optical coupler using an imaging lens. Although the scanning operation is digital, the driving system is relatively simple and multiple beams can be simultaneously generated by selecting multiple output couplers. In this study, we discuss the port-selective-type beam scanning device.

Here, we describe the operation mechanism of the port-selective optical beam scanner. Figure 3 shows the schematic image of the system. The output lights from the

coupler array are collimated through the imaging lens when the coupler array is on the focal plane of the lens, and then the beam is deflected to pass through the opposite focal point of the lens. The beam spot size at the lens position is expressed as

$$D_{\mathrm{b}} = D_{\mathrm{c}} + 2f\tan\theta_{\mathrm{c}} \tag{1}$$

where, D_{c} and θ_{c} are beam spot size and divergence angle emitted from the coupler, respectively, and f is the focal length of the imaging lens. The spot size is decreased by introducing a lens with a small f and optical couplers with a small θ_{c}. Next, the beam scanning angular resolution θ_{res} and field of view (FOV) angle θ_{FOV} are expressed as

$$\begin{aligned}\theta_{\mathrm{res}} &= \theta_M - \theta_{M-1} \\ &= \arctan\left(\frac{f}{d\cdot M}\right) - \arctan\left\{\frac{f}{d(M-1)}\right\} \end{aligned} \tag{2}$$

$$\begin{aligned}\theta_{\mathrm{FOV}} &= 180 - 2\theta_M \\ &= 2\arctan\left(\frac{d\cdot M}{f}\right) \end{aligned} \tag{3}$$

where, d is the pitch of the arrayed couplers, M indicates the array order of couplers counted from the center coupler on the lens axis, and the total number of the arrayed couplers N is expressed by $2M+1$. Smaller d and longer f increase the scanning resolution but reduce the FOV. Although the FOV can be widened by increasing the M, there is a physical limit to the number of optical couplers that can be integrated into a device chip. These structural parameters should be determined according to the requirements of the FSO communication application.

2.3 Design for Indoor FSO Communication

Then, we consider indoor mobile FSO communication as one of the use cases. The beam scanners are expected to be installed on the ceiling of a room, as shown in Fig. 4 (a). Because the deflection angle of the output beam changes digitally, if the device is designed so that the beam collimates,

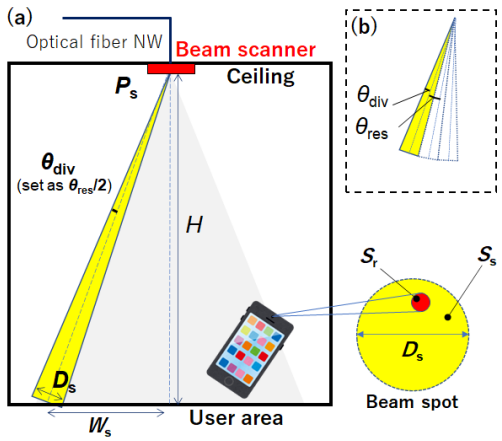

Fig. 4 Schematic image of indoor mobile FSO communication.

the dark areas will appear on the user area where the optical spots do not overlap, resulting in communicating disconnection. To avoid this, the output beam requires some divergence [1], [5]. For example, if the beam divergence angle θ_{div} is set to half of the scanning resolution, then the optical received power in the user area can be maintained within a 3 dB bandwidth in the array direction, regardless of the ceiling height, as shown in Fig. 4 (b). However, divergent light decreases the optical power density over the user area, leading to a reduction of the received optical power. Thus, the design of the entire system, including the receiver, must be optimized.

Next, we discuss the theoretical optical power density at the user area to provide the design guideline for the indoor mobile FSO communication system. In this calculation, the divergence angle was set as half of the scanning resolution. The position reached on the user area by the beam emitted from the coupler M and the spot size at the position are expressed by the following equations.

$$\begin{aligned}W_{\mathrm{s}} &= H\cdot\tan\left(\frac{\theta_{\mathrm{FOV}}}{2}\right) \\ &= H\cdot\tan\left\{\arctan\left(\frac{d\cdot M}{f}\right)\right\} \\ &= \frac{d\cdot M\cdot H}{f} \end{aligned} \tag{4}$$

$$\begin{aligned}D_{\mathrm{s}} &= D_{\mathrm{b}} + 2\sqrt{H^2+W_s^2}\tan\theta_{\mathrm{res}} \\ &\approx 2\sqrt{H^2+\left(\frac{d\cdot M\cdot H}{f}\right)^2}\tan\left[\arctan\left(\frac{f}{d\cdot M}\right)\right. \\ &\quad \left. -\arctan\left\{\frac{f}{d(M-1)}\right\}\right] \end{aligned} \tag{5}$$

where, H is the height of the ceiling. For the indoor FSO application, the D_{b} is negligibly smaller than D_{s} because the beam spot is sufficiently spread during propagation over a long distance. The received power at the user area is expressed as

$$\begin{aligned}P_{\mathrm{r}}\,[\mathrm{dBm}] &= P_s + 10\log_{10}\left(\frac{S_{\mathrm{r}}}{S_{\mathrm{s}}}\right) \\ &= P_s + 10\log_{10}\left\{\frac{S_{\mathrm{r}}}{\pi\left(\frac{D_{\mathrm{s}}}{2}\right)^2}\right\} \end{aligned} \tag{6}$$

where, S_{s} and S_{r} are the beam-spot area and receiver's aperture area, and P_{s} is the optical intensity of the output beam emitted from the optical coupler. From Eq. (6), the received power can be increased by i) increasing P_{s}, ii) increasing S_{r}, and iii) narrowing D_{s}.

Figure 5 (a) shows the received power as a function of the user position for each output power. The eye safety standards allow optical emission intensity of up to 10 dBm for infrared beams with wavelengths > 1400 nm [5]. The coupler array pitch and focal length of the lens were fixed at 50 μm and 7.5 mm, respectively, which corresponds to the

device parameters described in Sect. 3. The ceiling height and aperture size of the receiver were assumed to be 5 m and 4 mm^2, respectively. As shown in the graph, the received power increases in proportion to the optical power. The dashed guidelines in Fig. 5 (a) indicate the irradiation positions on the user area for the output beams from each optical coupler. The irradiation positions for the couplers with M = 32 and 64 were 1.07 and 2.13 m, respectively.

Figure 5 (b) shows the aperture size dependence of the received power for the receiver, and the received power increased in proportion to the area. However, receivers with a large-aperture photodiode are generally not suitable for high-speed signal reception because of their slow response time, and thus, technologies are required to efficiently focus the diverged light onto a small photodiode for the receiver.

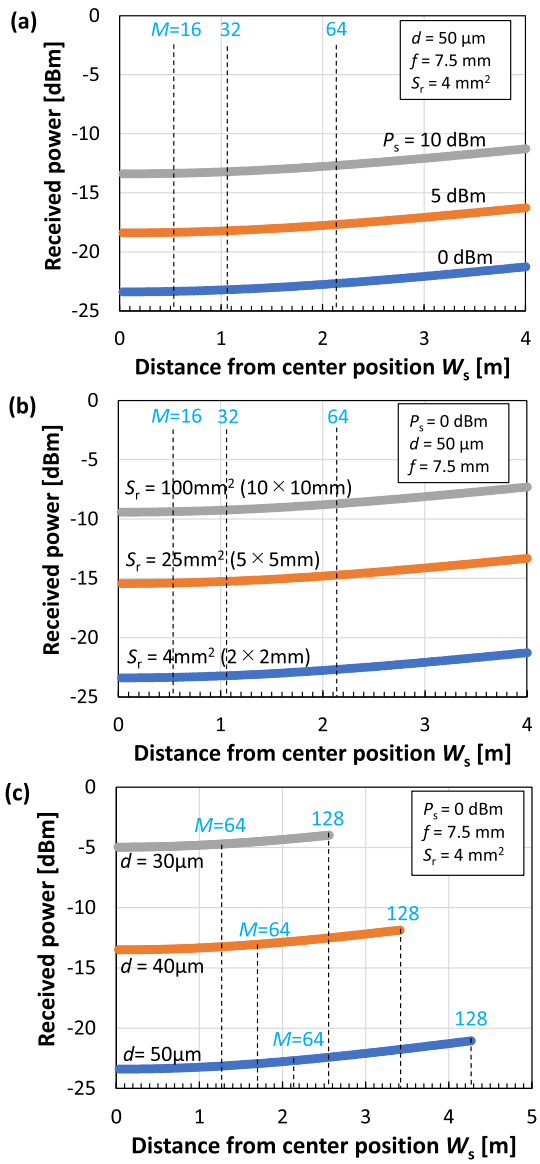

Fig. 5 User position dependence of received power for each design parameter. (a) Optical beam intensity. (b) Receiver footprint. (c) Optical coupler pitch.

Figure 5 (c) shows the coupler pitch dependence of the received power. The narrow pitch leads to a small scanning resolution, as expected from Eq. (2). Therefore, the beam size D_s becomes small because the divergence angle was set as half of the scanning resolution, and the received power increased. However, the beam scanning area on the user area simultaneously becomes small, and the number of coupler arrays must be increased to widen the FOV; otherwise, multiple beam scanning devices must be installed on the ceiling to enlarge the coverage area.

The required receiving power for the signal communication depends on the modulation format and modulation speed of the optical signal. We expect that increasing the number of wavelength channels by introducing a broadband elephant coupler can increase the communication capacity while keeping the modulation speed low, thereby increasing the flexibility in FSO system specifications.

3. Device Structure and Fabrication

We developed the prototype silicon beam scanning device shown in Fig. 2 [20], [21]. This device was designed for TE polarization, and elephant couplers with an optical beam spot size of 5 µm are incorporated for the optical input and output. The light input from the coupler passes through the thermo-optic MZ switches arranged in a seven-stage tournament-tree configuration, which selectively outputs 128 optical paths (i.e., 1 × 128 optical path switch), leading to the 8 × 16 matrix elephant coupler array with a pitch of 50 µm. We have previously demonstrated high-performance large-scaled optical matrix switching systems (e.g., 32 × 32 strictly-non-blocking silicon path-independent insertion-loss switches) [29]–[31], and in this present work, we utilized the element technology in the device.

The silicon photonics chip integrating the optical path-switching system was fabricated by argon fluoride (ArF) immersion lithography using a 300 mm CMOS pilot line at AIST-SCR. Then, after dicing into small chips, the elephant coupler was formed according to the fabrication process shown in Fig. 6. First, both the SiO_2 over-cladding and 3 µm-thick BOX layer surrounding the Si waveguide terminals that becomes the elephant coupler were partially removed by dry-etching and subsequent wet-etching processes using a buffered hydrofluoric (BHF) acid solution.

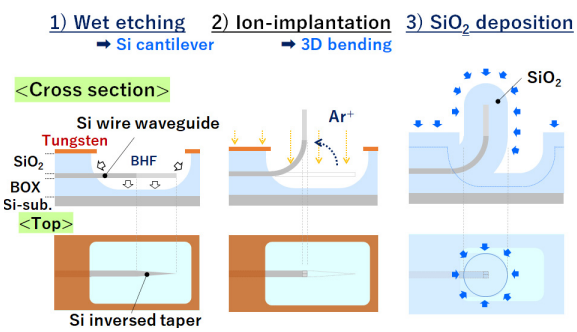

Fig. 6 Schematic image of the elephant coupler fabrication process.

The cross-sectional dimensions of the Si wire waveguide were designed to be 430 × 220 nm, and the width exponentially narrows down to 50 nm for the inversed taper. Then, the cantilevered Si waveguides were three-dimensionally bent by Ar^+ implantation under an acceleration voltage of 110 keV and a beam current of 50 μA, where stress distribution within the cantilevered Si waveguide is generated because of the lattice defects. In this process step, the area other than the cantilevered waveguide was shielded with a tungsten mask to avoid unwanted ion irradiation. The mask also enhances the uniformity and reproducibility of the bent shape. Thus, a waveguide-tip position accuracy of less than ± 0.4 μm has been obtained [26]. Finally, the SiO_2 cladding with a dome-like coupler top was formed on the curved waveguides by executing isotropic SiO_2 deposition using the TEOS-PECVD process. The thickness of the cladding was approximately 3 μm, which enables the 5μm-spot collimated beam.

Figure 7 shows images of the fabricated devices. The footprints of the device chip and optical couplers array were 11 × 5 mm^2 and 750 × 350 μm^2, respectively. The quality of the elephant coupler array was confirmed by scanning electron microscopy (SEM), as shown in Fig. 7 (b). The device chip was electrically mounted on a printed circuit board using wire bonding, as shown in Fig. 7 (c). In the fabricated device, some of the optical switches did not work because the electrical wires were partially damaged during the BHF wet-etching process, and not all couplers could output optical beams. Therefore, in this work, we discuss the optical characteristics using the results of the measurable ports. This fabrication problem may be solved by refining the wet-etching process.

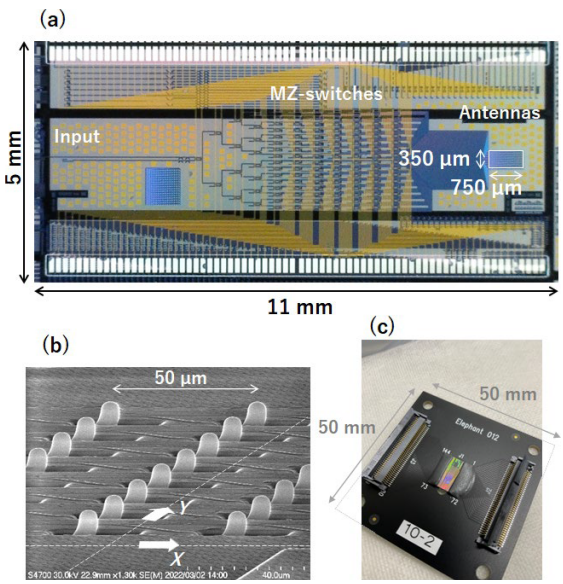

Fig. 7 Images of fabricated device: (a) Optical microscopic image of the device chip. (b) SEM image of the coupler arrays. (c) Electrical mounting samples [20], [21]

4. Measurement

4.1 On-Chip Characteristics

First, we evaluated the beam vector and beam divergence angle from the elephant couplers [20]. In this measurement, a TE-polarized amplified spontaneous emission (ASE) light in the wavelength range of 1530 to 1610 nm was input to the device through the tip-lensed polarization maintained optical fiber (PMF) with a spot size of 5 μm, and the optical intensity profile of the emitted beam from the coupler was measured for each sensor height. As the result, the beam vectors were tilted from the vertical axis and measured to be 10.8° and 1.2° for the X- and Y-axes in Fig. 7 (b), respectively. This is because the dosage of ion implantation was inappropriate. The divergence angles of the beam were measured to be 12.1° and 11°, respectively, which are close to the theoretical value of 11.3° for a 5 μm-spot Gaussian beam. A Gaussian-like beam enables beam scanning operation using a simple mass-product imaging lens, which contributes to lower module cost.

Next, the transmission loss of the device chip was evaluated. Figure 8 (a) shows the measurement setup. We measured the loss by varying the tilt angles of the input and output optical fibers. Figure 8 (b) shows the transmission spectra. The loss includes the coupling losses for input and output and device loss. A minimum loss value of 5.6 dB was obtained when the fiber angle was set to 11°, which is consistent with the above-mentioned beam vector [21]. According to the previous work, the insertion losses of the MZ-switch element and waveguide propagation loss were estimated to be 0.16 dB/unit and 1.2 dB/cm, respectively, and the on-chip loss was assumed to be approximately 2.3 dB [29], [30]. Therefore, the total coupling loss of the

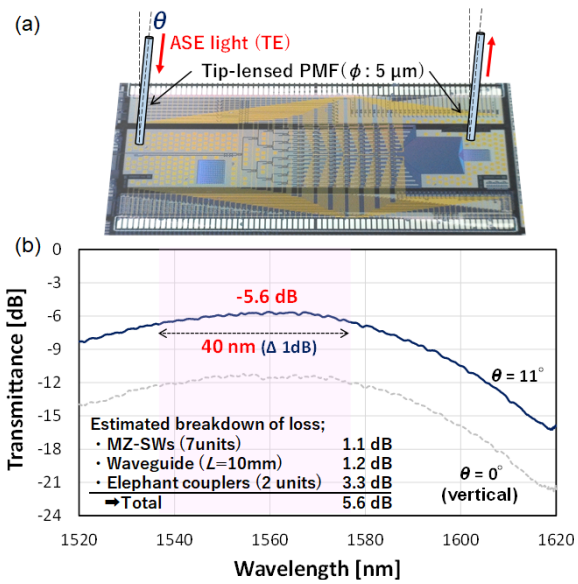

Fig. 8 Fiber-to-fiber optical transmission through the beam scanning device: (a) Measurement set up. (b) Measured spectra [21].

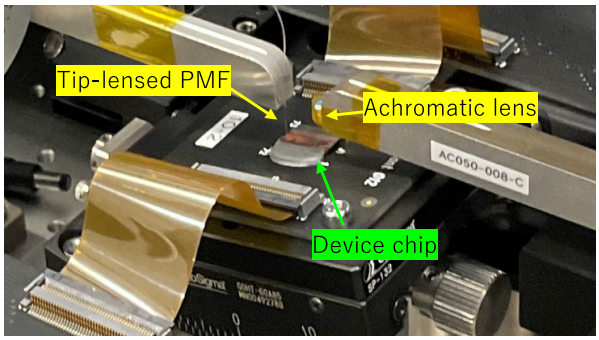

Fig. 9 Measurement setup for beam scanning operation.

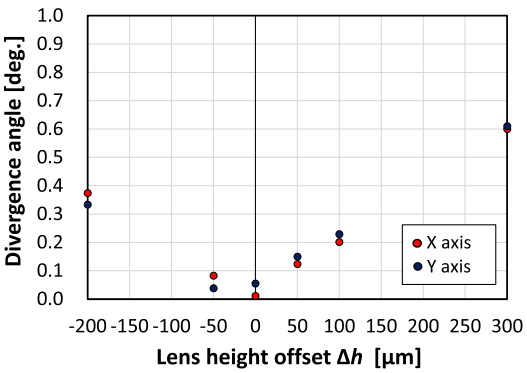

Fig. 10 Measured beam divergence angle as a function of lens height. The reference position of the lens is at the focal point of the lens [21].

input and output was estimated to be 3.3 dB, (i.e., 1.65 dB/coupler). Furthermore, broadband operation with a 1 dB-loss bandwidth of 40 nm was obtained. The bandwidth was determined based on the cumulative bandwidth of the input/output elephant couplers and the seven cascaded MZ switches, where the bandwidth of the single elephant coupler was over 180 nm according to the previous work [25].

4.2 Beam Scanning Characteristics

The beam scanning operation was examined by introducing an imaging lens. Figure 9 shows the experimental setup. A commercial achromatic lens (Thorlabs: AC050-008-C) with a focal length of 7.5 mm and a lens diameter of 5 mm was positioned above the device. The device was placed on the sample mount with an 11° tilt so that the output beam from the elephant coupler was perpendicular to the measurement system. The same ASE light source with a wavelength range from 1530 to 1610 nm was used as the input light.

Figure 10 shows the divergence angle as a function of lens height [21]. We obtain the minimal divergence beam with 0.01° and 0.05° for the X- and Y-axes, respectively, around the focal position. Thus, we successfully formed a wavelength-insensitive diverged beam over a wavelength range of at least 80 nm using the elephant couplers. Such a wavelength-insensitive beam is more useful for broadband signal transmission compared to the grating couplers with relatively high wavelength sensitivity. For the FSO communication, we need to use a diverged beam, as described in Sect. 2, which can be generated by applying the height offset to the lens position, as shown in Fig. 10. The small difference in the lens height, offering minimal divergence between X- and Y-axes, might result from the difference in the beam waist positions of the elephant couplers.

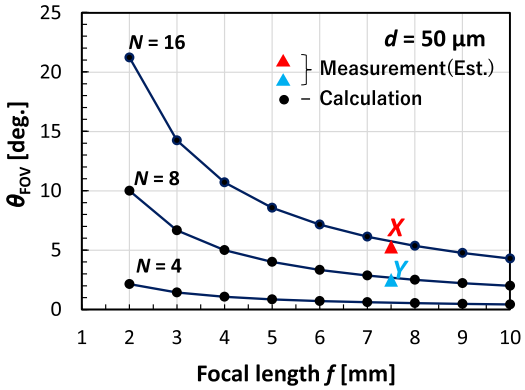

Fig. 11 Focal length dependence of the FOV.

Next, the beam scanning resolution and FOV were measured [21]. The output port was changed by operating the MZ switches. The beam scanning resolution was measured to be 0.35° and 0.36° for the X- and Y-axes, respectively, which almost matched the theoretical result of 0.38° calculated using Eq. (2), where the d, f, and M are 50 μm, 7.5 mm, and 1, respectively. The FOV with 16 and 8 arrayed couplers was estimated from the experimental scanning resolution to be 5.3° and 2.5° for the X- and Y-axes, respectively. Figure 11 shows the calculated focal length dependence of the FOV using Eq. (3), with the experimental estimation in the triangle plots. The FOV can be increased by shortening the focal length or increasing the number of couplers.

4.3 Free-Space Signal Transmission

Finally, the free-space signal transmission was performed using the fabricated beam scanning device [21]. Figure 12 shows the experimental setup for evaluating the signal transmission for each coupler output. A pluggable optical transceiver (GigaLight: 10G SFP+ AOC Checker) was used to measure the bit error rates (BERs), where a 10 Gbps pseudo-random binary sequence (PRBS) signal in NRZ-OOK format, with a pattern length of $2^{31}-1$ and wavelength of 1550 nm, was generated and received. The tip-lensed optical fiber was used for optical input, and the achromatic lens was set above the device so that the beam divergence angle was minimized (quasi-collimation), using the configuration described in Sect. 4.2, where the optical beam spot size was 2.02 and 1.89 mm for the X- and Y-axes, respectively. The distance of free-space transmission was 10 cm, which was the maximum distance for the present experimental setup. On the receiver side, an optical fiber collimator (Thorlabs: TC12FC-1550) was introduced to couple the beam into a single-mode fiber, where the position and axis

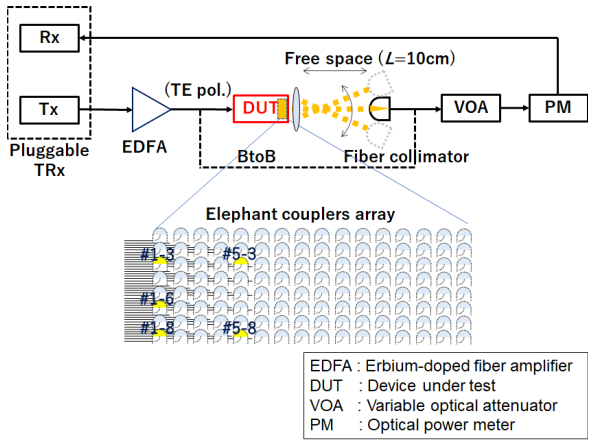

Fig. 12 Experimental setup for signal transmission using the developed beam scanner. The axis of the achromatic lens was set to the coupler of #1–3.

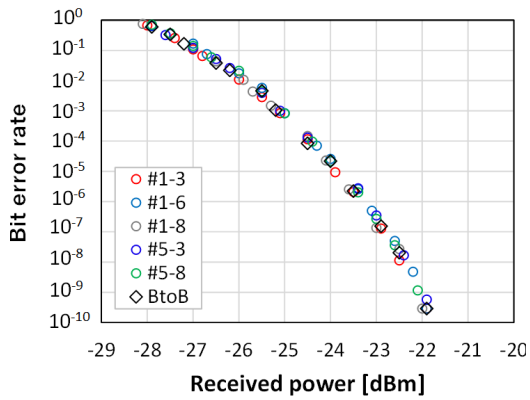

Fig. 13 10 Gbps NRZ-OOK signal transmission for each output coupler [21].

of the collimator were aligned with each beam by optical power monitoring. Figure 13 shows the result. Each label corresponds to the coupler number described in Fig. 12. The power penalty foreach port to the back-to-back (BtoB) measurement was negligibly small, and thus, signal degradation was not observed.

Next, the wavelength characteristics were evaluated using the measurement setup shown in Fig. 14. At the transmitter, a tunable laser (Santec: TSL-550) was used for the light source, and 10 Gbps NRZ-OOK signals with a PRBS of $2^{15} - 1$ were generated. In this experiment, the output coupler of #1–3 was used for signal transmission. Figure 15 shows the measured power penalty at the BER of 10^{-9} for each signal wavelength in the wavelength range from 1530 to 1590 nm, which was a little wider than the 1dB-loss bandwidth of the device chip shown in Fig. 8. There were also small power penalties with < 0.11 dB for each wavelength channel in the BtoB measurement, which was almost the same as the light intensity variation caused by input fiber fluctuations. The wide wavelength signal transmission was achieved because of the broadband elephant couplers. To the best of our knowledge, this is the first report of free-space

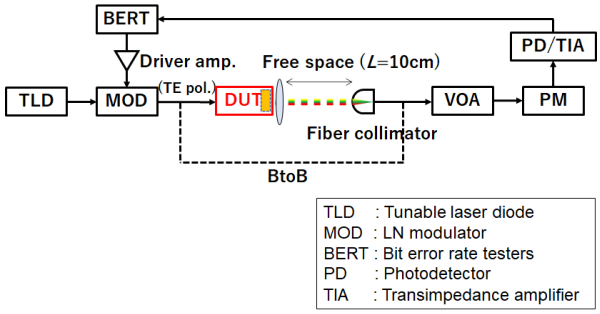

Fig. 14 Experimental setup for signal transmission.

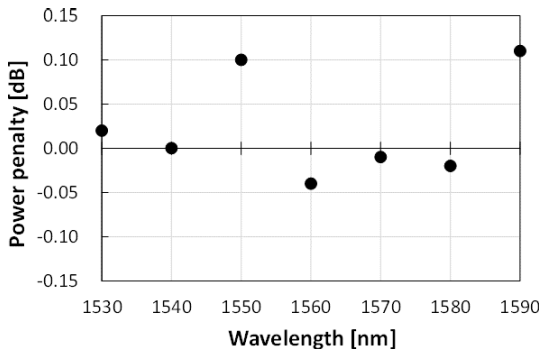

Fig. 15 Measured power penalty for the BtoB at the BER of 10^{-9} as a function of signal wavelength.

signal transmission in such a wide wavelength range using a 2D silicon photonics beam scanning device.

5. Conclusion

In this paper, we presented the overview of broadband port-selective beam scanning device incorporating elephant couplers for FSO communication systems as the complements of the conference proceedings [20], [21]. First, using the theoretical calculation of the optical power density at the user area, the design guidelines for indoor mobile FSO communication systems were discussed. Next, we showed the prototype of the beam scanning device fabricated partly using the 300 mm CMOS pilot line and the lab-level experimental facilities. The fabricated device showed a 1dB bandwidth of 40 nm and an insertion loss of 5.6 dB, which were obtained using the fiber-to-fiber measurement. Then, the optical beam properties were evaluated after passing through the achromatic lens, and a diverged wavelength-insensitive beam was obtained over a wavelength range of 80 nm, owing to the broadband property of the elephant coupler. Moreover, the beam scanning resolution and FOV were evaluated using the MZ switch. Finally, 10 Gbps NRZ-OOK signal transmission at a free-space distance of 10 cm was successfully performed with a small power penalty over a wavelength range of 60 nm. Such a broadband 2D beam scanning device may be useful in next-generation mobile communication systems.

Acknowledgments

These research results were obtained from commissioned research conducted by the National Institute of Information and Communications Technology (NICT), JAPAN, and also financially supported by the Japan Society for the Promotion of Science (JSPS) under a Grant-in-Aid for Scientific Research (#20K04634).

References

[1] Y. Kaymak, R. Rojas-Cessa, J. Feng, N. Ansari, M. Zhou, and T. Zhang, "A survey on acquisition, tracking, and pointing mechanisms for mobile free-space optical communications," IEEE Commun. Surv. Tutor., vol.20, no.2, pp.1104–1123, 2018.

[2] A. Dogra, R.K. Jha, and S. Jain, "A survey on beyond 5G network with the advent of 6G: architecture and emerging technologies," IEEE Access, vol.9, no.3, pp.67512–67547, 2021.

[3] K. Wang, Z. Yuan, E. Wong, K. Almach, H. Li, K. Sithamparanathan, and E. Skafidas, "Experimental demonstration of indoor infrared optical wireless communications with a silicon photonic integrated circuit," J. Lightw. Technol., vol.37, no.2, pp.619–626, 2019.

[4] H.-W Rhee, J.-B. You, H. Yoon, K. Han, M. Kim, B.G. Lee, S.-C. Kim, and H.-H. Park, "32 Gbps data transmission with 2D beam-steering using a silicon optical phased array," IEEE Photon. Technol. Lett., vol.32, no.13, pp.803–806, 2020.

[5] T. Koonen, F. Gomez-Agis, F. Huijskens, K.A. Mekonnen, Z. Cao, and E. Tangdiongga, "High-capacity optical wireless communication using two-dimensional IR beam steering," J. Lightw. Technol., vol.36, no.19, pp.4486–4493, 2018.

[6] K. Wang, "Remote-powered infrared indoor optical wireless communication systems," IEEE Photon. Technol. Lett., vol.34, no.9, pp.455–458, 2022.

[7] H. Elgala, R. Mesleh, and H. Haas, "Indoor optical wireless communication: potential and state-of-the-art," IEEE Commun. Mag., vol.49, no.9, pp.56–62, 2011.

[8] K. Wang, "Quasi-Passive Indoor Optical Wireless Communication Systems," IEEE Photon. Technol. Lett., vol.32, no.21, pp.1373–1376, 2020.

[9] A. Gomez, K. Shi, C. Quintana, M. Sato, G. Faulkner, B.C. Thomsen, and D. O'Brien., "Beyond 100-Gb/s indoor wide field-of-view optical wireless communications," IEEE Photon. Technol. Lett., vol.27, no.4, pp.367–370, 2015.

[10] T.K. Chan, M. Megens, B.-W. Yoo, J. Wyras, C.J. Chang-Hasnain, M.C. Wu, and D.A. Horsley, "Optical beamsteering using an 8 × 8 MEMS phased array with closed-loop interferometric phase control," Opt. Express vol.21, no.3, pp.2807–2815, 2013.

[11] D. Inoue, T. Ichikawa, A. Kawasaki, and T. Yamashita, "Demonstration of a new optical scanner using silicon photonics integrated circuit," Opt. Express, vol.27, no.3, pp.2499–2508, 2019.

[12] H. Ito, Y. Kusunoki, J. Maeda, D. Akiyama, N. Kodama, H. Abe, R. Tetsuta, and T. Baba, "Wide beam steering by slow-light waveguide gratings and a prism lens," Optica, vol.7, no.1, pp.47–52, 2020.

[13] C.V. Poulton, M.J. Byrd, P. Russo, E. Timurdogan, M. Khandaker, D. Vermeulen, and M.R. Watts, "Long-range LiDAR and free-space data communication with high-performance optical phased arrays," IEEE J. Sel. Topics Quantum Electron., vol.25, no.5, Art no.7700108, pp.1–8, 2019.

[14] X. Zhang, K. Kwon, J. Henriksson, J. Luo, and M.C. Wu, "A large-scale microelectromechanical-systems-based silicon photonics LiDAR," Nature, vol.603, pp.253–258, 2022.

[15] Y.-C. Chang, M.C. Shin, C.T. Phare, S.A. Miller, E. Shim, and M. Lipson, "2D beam steerer based on metalens on silicon photonics," Opt. Express, vol.29, no.2, pp.854–864, 2021.

[16] A. Bozzola, L. Carroll, D. Gerace, I. Cristiani, and L.C. Andreani, "Optimising apodized grating couplers in a pure SOI platform to −0.5 dB coupling efficiency," Opt. Express, vol.23, no.12, pp.16289–16304, 2015.

[17] W.D. Sacher, Y. Huang, L. Ding, B.J.F. Taylor, H. Jayatilleka, G.-Q. Lo, and J.K.S. Poon, "Wide bandwidth and high coupling efficiency Si_3N_4-on-SOI dual-level grating coupler," Opt. Express, vol.22, no.9, pp.10938–10947, 2014.

[18] L. Carroll, D. Gerace, I. Cristiani, and L.C. Andreani, "Optimizing polarization-diversity couplers for Si photonics: reaching the −1dB coupling efficiency threshold," Opt. Express, vol.22, no.12, pp.14769–14781, 2014.

[19] X. Mu., S. Wu, L. Cheng, and H.Y. Fu, "Edge couplers in silicon photonic integrated circuits: A review," Appl. Sci., vol.10, no.4, p.1538, 2020.

[20] Y. Atsumi, T. Yoshida, R. Matsumoto, R. Konoike, Y. Sakakibara, T. Inoue, and K. Suzuki, "Demonstration of port-selective beam scanner incorporating silicon vertically curved waveguide antenna arrays," Proc. OECC/PSC, no.TuE4-2, Toyama, Japan, 2022.

[21] Y. Atsumi, T. Yoshida, R. Matsumoto, R. Konoike, Y. Sakakibara, T. Inoue, and K. Suzuki., "Free-space signal transmission using optical beam scanning device incorporating broadband silicon surface optical couplers," Proc. Optical Fiber Communication Conf. (OFC), no.M3C.4, San Diego, Japan, 2023.

[22] T. Yoshida, S. Tajima, R. Takei, M. Mori, N. Miura, and Y. Sakakibara, "Vertical silicon waveguide coupler bent by ion implantation," Opt. Express, vol.23, no.23, pp.29449–29456, 2015.

[23] T. Yoshida, E. Omoda, Y. Atsumi, T. Nishi, S. Tajima, N. Miura, M. Mori, and Y. Sakakibara, "Vertically curved Si waveguide coupler with low loss and flat wavelength window," J. Lightw. Technol., vol.34, no.7, pp.1567–1571, 2016.

[24] Y. Atsumi, T. Yoshida, E. Omoda, and Y. Sakakibara, "Design of compact surface optical coupler based on vertically curved silicon waveguide for high-numerical-aperture single-mode optical fiber," Jpn. J. Appl. Phys., vol.56, no.9, p.090307, 2017.

[25] T. Yoshida, Y. Atsumi, E. Omoda, and Y. Sakakibara, "Polarization-insensitive vertically curved Si surface optical coupler bent by ion implantation," IEEE Photon. Technol. Lett., vol.32, no.20, pp.1319–1322, 2020.

[26] T. Yoshida, Y. Atsumi, E. Omoda, and Y. Sakakibara, "Improvement of fabrication accuracy of vertically curved silicon waveguide optical coupler using hard mask shielded ion implantation bending," Jpn. J. Appl. Phys., vol.59, no.7, p.078003, 2020.

[27] Y. Atsumi, T. Yoshida, and Y. Sakakibara, "Design of aspherical-lensed Si surface optical coupler for coupling with standard single-mode optical fibers," Jpn. J. Appl. Phys., vol.59, no.10, p.100905, 2020.

[28] T. Amemiya, T. Yoshida, Y. Atsumi, N. Nishiyama, Y. Miyamoto, Y. Sakakibara, and S. Arai, "Orbital angular momentum Mux/Demux module using vertically curved Si waveguides," Proc. Optical Fiber Communication Conf., San Diego, CA, no.M1C.7, 2019.

[29] K. Suzuki, R. Konoike, J. Hasegawa, S. Suda, H. Matsuura, K. Ikeda, S. Namiki, and H. Kawashima, "Low insertion loss and power efficient 32 × 32 silicon photonics switch with extremely-high-Δ PLC connector," J. Lightw. Technol., vol.37, no.1, pp.116–122, 2018.

[30] K. Suzuki, R. Konoike, S. Suda, H. Matsuura, S. Namiki, H. Kawashima, and K. Ikeda, "Low-loss, low-crosstalk, and large-scale optical switch based on silicon photonics," J. Lightw. Technol., vol.38, no.2, pp.233–239, 2020.

[31] R. Matsumoto, R. Konoike, K. Suzuki, H. Matsuura, K. Ikeda, T. Inoue, and S. Namiki, Proc. Optical Fiber Communication Conf. (OFC), San Diego, CA, no.Tu6A.2, 2021.

Yuki Atsumi received the B.E., M.E., and Ph.D. degrees in Electrical and Electronic Engineering from Tokyo Institute of Technology, Japan, in 2009, 2011, and 2013, respectively. He joined the National Institute of Advanced Industrial Science and Technology (AIST) in 2014. He is a member of the Japan Society of Applied Physics, IEICE, and IEEE Photonics Society. His research interest is in silicon photonics including heterogenous material integration.

Tomoya Yoshida received the B.E. and M.E. degrees in Electrical Engineering from Kyushu Institute of Technology, Iizuka, Japan, in 2002 and 2004, and the Ph. D degree in Electrical Engineering from Kyushu University, Ito, Japan, in 2007. Since 2007, he studies ion implantation bending (IIB) technology and its application to form the three-dimensional micro-scale structure for electronics and photonics devices at the National Institute of Advanced Industrial Science and Technology (AIST), Tsukuba, Japan. From 2017 to 2018, he was a Deputy Director of the Information Technology Industry Division of the Ministry of Economy, Trade, and Industry, in Japan. He is presently a senior researcher with AIST. His current research interests are in the optical coupler of silicon photonics. He is a member of the IEEE Photonics Society, the Japan Society of Applied Physics, and the Institute of Electronics, Information, and Communication Engineers of Japan.

Ryosuke Matsumoto received the B.E., M.E., and Ph.D. degrees in communication engineering from Osaka University, Osaka, Japan, in 2012, 2013, and 2016, respectively. From 2016 to 2019, he worked for the Mitsubishi Electric Corporation on optical access system and digital coherent transmission. In 2019, he joined the National Institute of Advanced Industrial Science and Technology (AIST), Japan, where he is currently working on optical switch system for data center networks. He is a member of IEICE and IEEE Photonics Society.

Ryotaro Konoike received M.E. and Ph.D. degrees from the Department of Electronic Science and Engineering, Kyoto University, Japan, in 2014 and 2017, respectively. He joined National Institute of Advanced Industrial Science and Technology (AIST), Japan in 2017. He is a member of JSAP, IEICE and IEEE. His research interests include silicon photonics and silicon optical switches.

Youichi Sakakibara The biography and photo are not available.

Takashi Inoue received his Ph.D. degree in communications engineering from Osaka University, Osaka, Japan, in 2002. He joined Furukawa Electric Co. Ltd., Ichihara, Japan, in 2002, where he developed optical signal processing devices based on nonlinear fiber optics, and silica-based planar lightwave circuits. In 2011, he joined National Institute of Advanced Industrial Science and Technology (AIST), Tsukuba, Japan, where he is currently working on digital coherent transmission systems, signal processing techniques, and optical networks. He is a member of the IEEE Photonics Society and the IEICE Communication Society.

Keijiro Suzuki received his BE and ME degrees from the Department of Electrical and Electronic Engineering, Shizuoka University, Hamamatsu, Japan, in 2004 and 2006, respectively. After spending two years at Sumitomo Osaka Cement Co., Ltd., he entered the Department of Electrical and Computer Engineering, Yokohama National University (YNU), Yokohama, Japan, in 2008 and was awarded the Research Fellowship for Young Scientists from JSPS. He received his Ph.D. degree from YNU in 2011. After spending one year at YNU as a post-doctoral fellow, he joined National Institute of Advanced Industrial Science and Technology (AIST), Tsukuba, Japan, in 2012. He is a member of the Optica, the IEICE, and the JSAP. His research interests include photonic integrated circuits, optical switches, and nonlinear optics.